EURASIP Journal on Wireless Communications and Networking

RESEARCH Open Access

Interleaved block subcarrier allocation and power combination for frequency symbol spreading multiuser diversity OFDMA

Yuta Ida[1*] and Takahiro Matsumoto[2]

*Correspondence:
y.ida@yamaguchi-u.ac.jp

[1] Graduate School of Sciences and Technology for Innovation, Yamaguchi University, Ube, Japan
[2] Graduate School of Science and Engineering, Kagoshima University, Kagoshima, Japan

Abstract

In a FSS-OFDMA, the OFDM symbol is spread, and the subcarriers are assigned for each user in the frequency band. As the principal subcarrier allocation for each user, localized and interleaved allocations have been proposed, and the interleaved allocation is improved for the BER performance to avoid continuous deep faded subcarrier channels. Also, in the independent channel fluctuation for each user, the MUDiv gain is obtained by the individual and block subcarrier allocations. However, they have a trade-off problem between the BER performance and the computational complexity. To solve this problem, the interleaved block subcarrier allocation has been proposed. On the other hand, the interleaved block is only evaluated for the individual subcarrier and is not evaluated for the several subcarriers. Moreover, the power combination between the subcarrier and the channel is also improved for the BER performance, but the individual and block subcarrier allocations are only evaluated. Therefore, in this paper, we propose the interleaved block subcarrier allocation and the power combination for a FSS-MUDiv/OFDMA.

Keywords: OFDMA, FSS, MUDiv, Interleaved block subcarrier allocation, Power combination

1 Introduction

1.1 Introduction

OFDM is very important technique to achieve high capacity transmissions by multicarrier systems [1]. Therefore, OFDM has been adopted in many standards such as WLAN, digital broadcasting, and mobile communication systems [2–4]. Also, as the access technique with an OFDM, OFDMA has been proposed and has been also adopted in these techniques. In recent access technique, OMA and NOMA are discussed [5]. In a NOMA, the capacity is expanded by assigning the signal for each user non-orthogonally, but the elaborate signal separation and detection such as the SIC are required. On the other hand, OFDMA is classified as an OMA, and the orthogonally between subcarriers and users is kept in the frequency band. Therefore, the signal separation and detection are achieved linearly such as the ZF and the MMSE. Moreover, in an OFDM, FSS-OFDM has been proposed and spreads the OFDM symbol by the spreading technique such as

the WHT and the DFT in the frequency band [6–9]. And then, in a FSS-OFDMA, the subcarrier allocation for each user is very important [10]. As the principal subcarrier allocation for each user, localized and interleaved allocations have been proposed. In the localized allocation, the subcarriers for each user are assigned continuously in the frequency band. This is a simple allocation. However, when continuous deep faded subcarrier channels occurred, the BER performance is deteriorated due to a burst error. On the other hand, in the interleaved allocation, the subcarriers for each user are assigned alternately in the frequency band [11–13]. In this case, the BER performance is improved compared with the localize allocation since a burst error is prevented by avoiding continuous deep faded subcarrier channels.

1.2 Related research status, problems, and this paper's contribution

In Table 1, the related research states, problems, and this paper fs contribution are summarized. In a wireless propagation channel, the channel fluctuation occurred due to a multipath fading at the frequency band [14]. And then, since the propagation channel for each user is independent, the channel fluctuation for each user is also independent. By using this characteristic, the MUDiv gain is obtained by assigning the subcarrier based on the CSI for each user [15]. In this paper, the subcarriers for each user are assigned based on the following condition that the number of subcarriers for each user is equal, and the BER performance is improved in all users. In this case, the individual and block subcarrier allocations have been proposed [16, 17]. The individual subcarrier allocation obtains the good BER performance compared with the block subcarrier allocation. However, large computational complexity is required. On the other hand, in the block subcarrier allocation, the block consists of the continuous several subcarriers, and the computational complexity is reduced. However, its BER performance is deteriorated compared with the individual subcarrier allocation. As a result, since they have a trade-off problem, we have proposed the following method to solve this problem [18–20]. As mentioned in Sect. 1.1, a burst error occurred due to a deep faded subcarrier channel. In [18], deep faded subcarrier channels are avoided by using cooperative communications, but several relay nodes are required. On the other hand, in [19, 20], the subcarriers for each user are assigned by the interleaved allocation as the same [11–13], and the MUDiv gain is obtained. In this case, deep faded subcarrier channels are avoided without cooperative communications. However, in [19], large computational complexity is required. Also, in [20], the interleaved block is

Table 1 Related research status, problems, and this paper's contribution

Method	Interleaved allocation	Flexibility	MUDiv gain	Computational complexity
Ref. [15]	X	X	O	Large
Refs. [16, 18, 21, 22]	X	O	O	Small to large
Refs. [11–13]	O	O	X	Small
Refs. [17, 19]	O	O	O	Large
Ref. [20]	O	X	O	Small
Refs. [23, 24]	X	O	X	Small
Proposed method	O	O	O	Small

only evaluated for the individual subcarrier, and its flexibility is not evaluated for the several subcarriers. Moreover, the power combination between the subcarrier and the channel has been proposed [21, 22]. It improves also the BER performance, but the individual and block subcarrier allocations are only evaluated. As the other method to solve a deep faded subcarrier channel, WF is also effective, but the adaptive threshold is required [23, 24]. Therefore, in this paper, we propose the interleaved block subcarrier allocation and the power combination for a FSS-MUDiv/OFDMA. The proposed method is the new FSS-OFDMA with the interleaved subcarrier allocation, and the utilization for the conventional FSS-OFDMA with the interleaved subcarrier allocation is introduced in the existing standards [9, 12, 13]. And then, since the proposed method is achieved by changing the subcarrier allocation method from the conventional method, authors think that the proposed method is compatible with existing standards.

1.3 Notation and this paper's organization

In Table 2, we define the notation for the symbols. And then, the rest of this paper is organized as follows. In Sect. 2, we present the system model for a FSS-MUDiv/OFDMA. Then, in Sect. 3, we indicate the methods for the conventional individual and block subcarrier allocations, and the proposed interleaved block subcarrier

Table 2 Notation for the symbols

B	Block length
$B_{\max}$	Maximum value of B
E_b	Energy per bit
$h_{u,l}$	Complex channel gain of the lth propagation path for the uth user
I	One chunk length for the interleaved block subcarrier allocation
$\mathcal{K}$	Constraint length
L	Discrete paths with the different time delay
N_0	Single side power spectral density
N_c	Number of subcarriers
N_d	Number of data symbols
N_{ici}	Power of the ICI
N_u	Number of users
$\tilde{N}_c$	$\lfloor N_c/N_u \rfloor$
R	Coding rate
S	Average transmission power
T_{wf}	Threshold for the WF
W_{wf}	Weight for the WF
$\tau_{u,l}$	Delay time of the lth propagation path for the uth user
$\Phi_{\tilde{N}_c}$	Spreading matrix for $(\tilde{N}_c \times \tilde{N}_c)$
$E[\cdot]$	Ensemble average operation
$\max(g)$	Maximum value of g
$\lfloor g \rfloor$	Integer lower and closer to g
$(\cdot)^*$	Complex conjugate operation
$(\cdot)^{-1}$	Inverse operation
$(\cdot)^T$	Transpose operation

allocation and power combination. And then, we discuss the system performance for the conventional and proposed methods by using the computer simulation in Sect. 4. Finally, we give the conclusion in Sect. 5.

2 System model

In this section, we indicate the system model for a FSS-MUDiv/OFDMA. Here, in Fig. 1, the block diagram of the proposed system is shown.

2.1 WHT and DFT

In a FSS-OFDM, the OFDM symbol is spread. In this paper, WHT and DFT are utilized as the spreading technique. WHT and DFT are expressed as the $(\tilde{N}_c \times \tilde{N}_c)$ matrix. Firstly, the WHT matrix is defined by

$$\mathbf{W}_{\tilde{N}_c} = \begin{bmatrix} \mathbf{W}_{\tilde{N}_c/2} & \mathbf{W}_{\tilde{N}_c/2} \\ \mathbf{W}_{\tilde{N}_c/2} & -\mathbf{W}_{\tilde{N}_c/2} \end{bmatrix}, \tag{1}$$

where $\mathbf{W}_1 = 1$. Next, the DFT matrix is defined by

$$\mathbf{F}_{\tilde{N}_c} = \begin{bmatrix} \omega^0_{\tilde{N}_c} & \omega^0_{\tilde{N}_c} & \cdots & \omega^0_{\tilde{N}_c} \\ \omega^0_{\tilde{N}_c} & \omega^1_{\tilde{N}_c} & \cdots & \omega^{\tilde{N}_c-1}_{\tilde{N}_c} \\ \vdots & \vdots & \ddots & \vdots \\ \omega^0_{\tilde{N}_c} & \omega^{\tilde{N}_c-1}_{\tilde{N}_c} & \cdots & \omega^1_{\tilde{N}_c} \end{bmatrix}, \tag{2}$$

where $\omega^k_{\tilde{N}_c} = \exp(-j2\pi k/\tilde{N}_c)$, and $j = \sqrt{-1}$.

2.2 Channel model

Firstly, the CIR for the uth user is constituted by

$$h_u(\tau) = \sum_{l=0}^{L-1} h_{u,l}\delta(\tau - \tau_{u,l}), \tag{3}$$

where $\sum_{l=0}^{L-1} E[|h_{u,l}|]^2 = 1$. And then, the CIR is converted to the CR by the FFT operation as

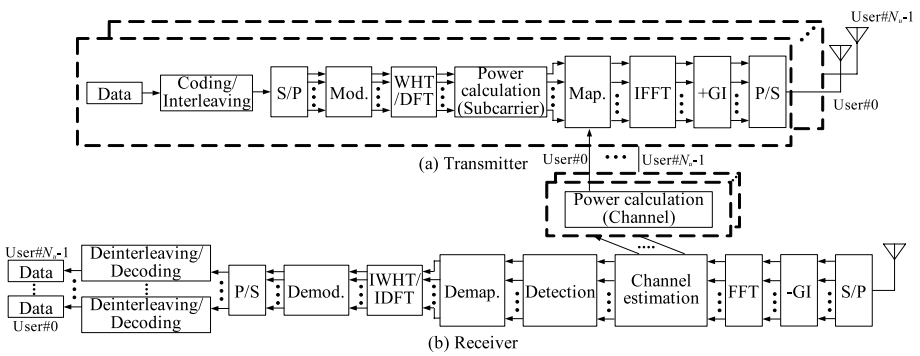

Fig. 1 Block diagram of the proposed system

$$H_u(k) = \int_0^{\infty} h_u(\tau) \exp(-j2\pi k\tau)\mathrm{d}\tau = \sum_{l=0}^{L-1} h_{u,l} \exp(-j2\pi k\tau_{u,l}). \tag{4}$$

2.3 Transmitter and receiver

Figure 1a shows the block diagram of the proposed system for the transmitter. Firstly, the original binary data signals are coded by the convolutional code with an interleaving. Next, after the S/P conversion, the parallel signals are modulated to $x_u(k,i)$ between the kth subcarrier and the ith symbol for the uth user. Here, its matrix form for the ith symbol is defined by

$$\mathbf{X}_u(i) = \left[x_u(0,i), \ldots, x_u(\tilde{N}_\mathrm{c}-1,i)\right]^\mathrm{T}. \tag{5}$$

In a FSS-OFDM, the ith OFDM symbol for Eq. (5) is spread by using $s_u(k,i)$ between the kth subcarrier and the ith symbol for the uth user as

$$\mathbf{S}_u(i) = \left[s_u(0,i), \ldots, s_u(\tilde{N}_\mathrm{c}-1,i)\right]^\mathrm{T} = \frac{1}{\sqrt{\tilde{N}_\mathrm{c}}} \Phi_{\tilde{N}_\mathrm{c}} \mathbf{X}_u(i). \tag{6}$$

Here, if $\Phi_{\tilde{N}_\mathrm{c}} = \mathbf{W}_{\tilde{N}_\mathrm{c}}$, the OFDM symbols are spread by the WHT. Also, if $\Phi_{\tilde{N}_\mathrm{c}} = \mathbf{F}_{\tilde{N}_\mathrm{c}}$, the OFDM symbols are spread by the DFT. After the symbol spreading, the spreading signals are mapped to the frequency band as

$$m_u(k,i) = \begin{cases} s_u(k,i) & \text{for } \gamma_u(k) = 1 \\ 0 & \text{for } \gamma_u(k) = 0, \end{cases} \tag{7}$$

where $\gamma_u(k)$ is the selection parameter as shown in Eq. (15). The mapping operation is indicated in Sect. 3. In the mapped signal, GI is inserted after the N_c points IFFT operation. Finally, after the P/S conversion, the time domain signal for the uth user is sent to the receiver as

$$m_u(t) = \sqrt{\frac{2S}{N_\mathrm{c}}} \sum_{i=0}^{N_\mathrm{d}-1} \sum_{k=0}^{N_\mathrm{c}-1} m_u(k,i) \exp\left(j2\pi \frac{kt}{N_\mathrm{c}}\right). \tag{8}$$

Figure 1b shows the block diagram of the proposed system for the receiver. Firstly, the time domain signal is given by

$$n(t) = \sum_{u=0}^{N_\mathrm{u}-1} \int_{-\infty}^{\infty} h_u(\tau) m_u(t-\tau)\mathrm{d}\tau + w(t), \tag{9}$$

where $w(t)$ is AWGN with a single side power spectral density of N_0. Next, after the S/P conversion and the GI elimination, the time domain signal is converted to the frequency domain signal by the N_c points FFT operation as

$$
\begin{aligned}
n(k,i) &= \sqrt{\frac{2S}{N_\mathrm{c}}} \sum_{t=iN_\mathrm{c}}^{(i+1)N_\mathrm{c}-1} n(t) \exp\left(-j2\pi \frac{kt}{N_\mathrm{c}}\right) \\
&= \sqrt{\frac{2S}{N_\mathrm{c}}} \sum_{u=0}^{N_\mathrm{u}-1} H_u(k,i) m_u(k,i) + w(k,i),
\end{aligned}
\tag{10}
$$

where $w(k,\ i)$ is AWGN with zero-mean and variance $2N_0/N_\mathrm{c}$. Here, we assume $H_u(k) = H_u(k,i)$ since $H_u(k,0) \approx H_u(k,1) \approx \cdots \approx H_u(k,N_\mathrm{d}-1)$. And then, the frequency domain signals are detected by using the weight $\omega(k)$ for the ZF or the MMSE and are demapped as

$$
\tilde{s}_u(k,i) = \omega(k)\gamma_u(k)n(k,i) = \begin{cases} \frac{\gamma_u(k)n(k,i)}{H_u(k)} & \text{for ZF} \\ \frac{\gamma_u(k)|H_u(k)|^* n(k,i)}{|H_u(k)|^2+N_0} & \text{for MMSE.} \end{cases}
\tag{11}
$$

Observing Eq. (11), the demapped signals for the uth user are obtained in $\gamma_u(k) = 1$, and its matrix form is expressed as

$$
\tilde{\mathbf{S}}_u(i) = \left[\tilde{s}_u(0,i), \ldots, \tilde{s}(\tilde{N}_\mathrm{c}-1,i)\right]^\mathrm{T}.
\tag{12}
$$

And then, the demapped signals are despread as

$$
\tilde{\mathbf{X}}_u(i) = \left[\tilde{x}_u(0,i), \ldots, \tilde{x}(\tilde{N}_\mathrm{c}-1,i)\right]^\mathrm{T} = \frac{1}{\sqrt{\tilde{N}_\mathrm{c}}} \Phi_{\tilde{N}_\mathrm{c}}^{-1} \tilde{\mathbf{S}}_u(i),
\tag{13}
$$

where $\tilde{x}_u(k,i)$ is the demapped signal for the uth user. Here, if $\Phi_{\tilde{N}_\mathrm{c}}^{-1} = \mathbf{W}_{\tilde{N}_\mathrm{c}}^{-1} = \mathbf{W}_{\tilde{N}_\mathrm{c}}$, the OFDM symbols are despread by the WHT. Also, if $\Phi_{\tilde{N}_\mathrm{c}}^{-1} = \mathbf{F}_{\tilde{N}_\mathrm{c}}^{-1}$, the OFDM symbols are despread by the IDFT. Finally, after the demodulation and the S/P conversion, the demodulated signals are decoded with a deinterleaving and are returned to the bit signals.

3 Methods

In this section, we indicate the methods for the conventional individual and block subcarrier allocations, and the proposed interleaved block subcarrier allocation and power combination. In this paper, as shown in Sect. 2, since $H_u(k,0) \approx H_u(1,i) \approx \cdots \approx H_u(k,N_\mathrm{d}-1)$, we assume $H_u(k) = H_u(k,i)$. Moreover, we assume also that the subcarriers for each user are not assigned in the same frequency band, and the number of subcarriers for each user is equal as $\tilde{N}_\mathrm{c}$. Additionally, Figs. 2, 4, and 5 show the example of the conventional and proposed subcarrier allocations for $N_\mathrm{c} = 8$ and $N_\mathrm{u} = 2$, and Fig. 3 shows the flowchart of the proposed interleaved subcarrier allocation and power combination.

3.1 Individual and block subcarrier allocations

As shown in Figs. 2, 4, and 5, in wireless communications, since the propagation channel for each user is independent, the channel fluctuation for each user is also independent at the frequency domain. By using this characteristic, the subcarriers for each user are assigned to obtain the MUDiv gain in the frequency band as

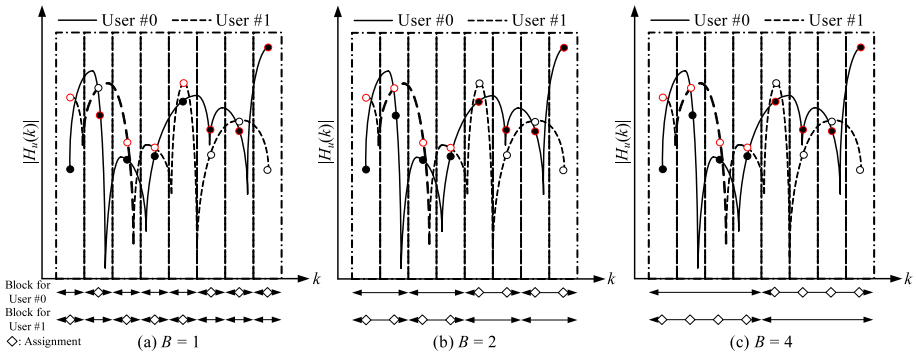

Fig. 2 Example of the conventional individual and block subcarrier allocations for $N_C = 8$, $N_U = 2$, and $B = 1$, 2, and 4

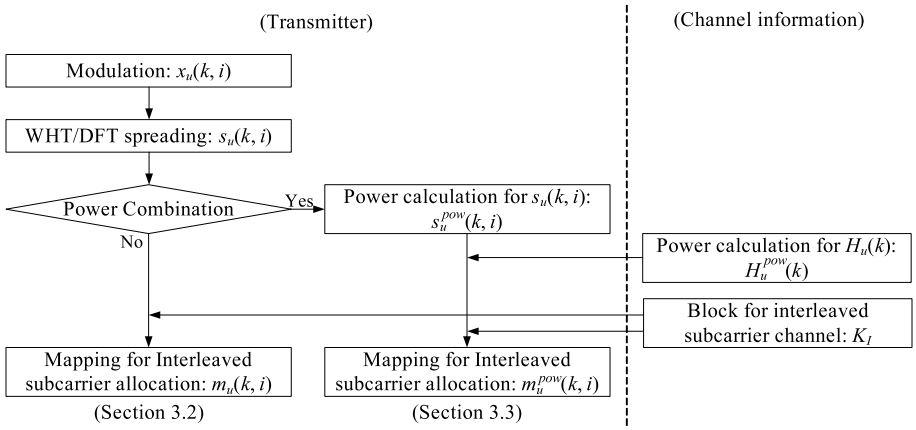

Fig. 3 Flowchart of the proposed interleaved block subcarrier allocation and power combination

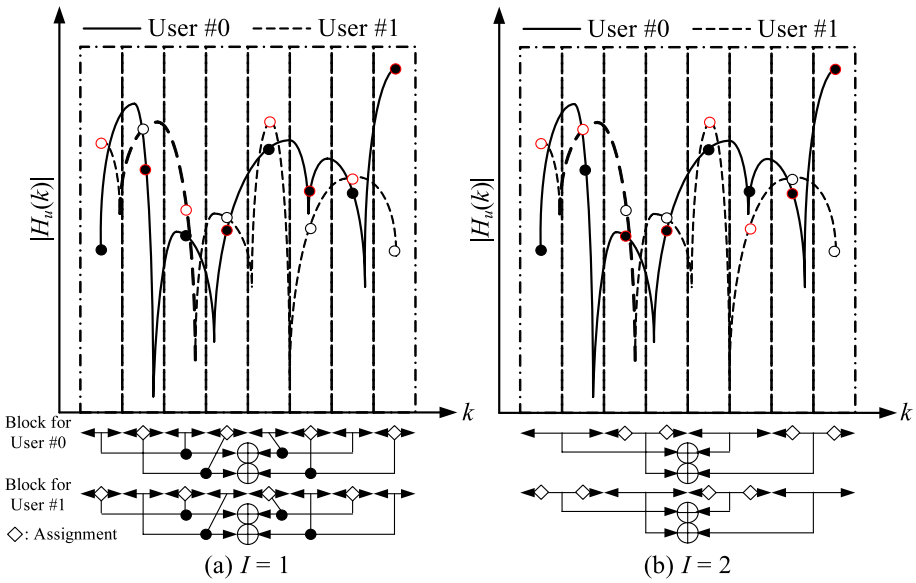

Fig. 4 Example of the proposed interleaved block subcarrier allocation for $N_C = 8$, $N_U = 2$, and $I = 1$and 2

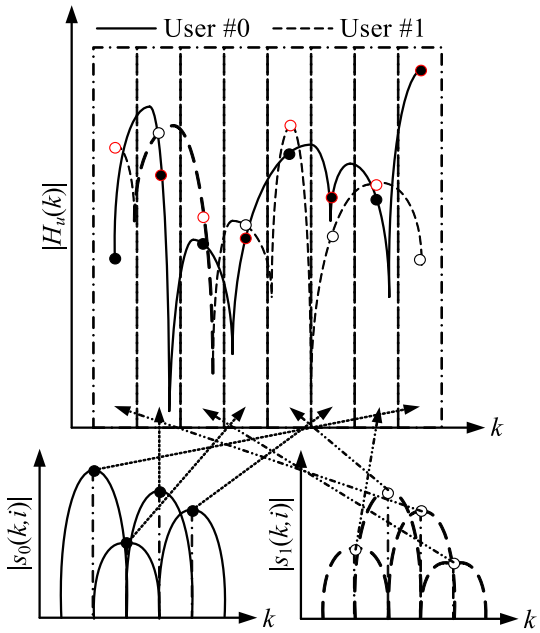

Fig. 5 Example of the proposed interleaved block subcarrier allocation and power combination for $N_c = 8$, $N_u = 2$, and $l = 1$

$$\begin{aligned} J_B &= \max\left(\sum_{\alpha=0}^{\lfloor N_c/B\rfloor^{N_u}-1} J_{B,\alpha}\right) = \max\left(\sum_{u=0}^{N_u-1}\sum_{k=0}^{\lfloor N_c/B\rfloor-1} |\mathcal{H}_{B,u}(k)|\gamma_u(k)\right) \\ &\le \sum_{u=0}^{N_u-1}\sum_{k=0}^{\lfloor N_c/B/N_u-1\rfloor} |\mathcal{H}_{B,u}^{\max}(k)|, \end{aligned} \tag{14}$$

where $\gamma_u(k)$ is the selection parameter as

$$\gamma_u(k) = \begin{cases} 1 & \text{for allocation} \\ 0 & \text{for no allocation,} \end{cases} \tag{15}$$

$\mathcal{H}_{B,u}^{\max}(k)$ is the subcarrier block channel which sorts the power of $\mathcal{H}_{B,u}(k)$ as $|\mathcal{H}_{B,u}^{\max}(0)| \ge \cdots \ge |\mathcal{H}_{B,u}^{\max}(\lfloor N_c/B\rfloor - 1)|$. $\mathcal{H}_{B,u}(k)$ is defined by Eq. (16). For Eq. (14), if the individual subcarrier allocation for $B = 1$, $\mathcal{H}_{1,u}(k) = H_u(k)$. In this case, at the example of Fig. 2a, J_B for $B = 1$ is given by

$$J_1 = |H_1(0)| + |H_0(1)| + |H_1(2)| + |H_1(3)| + |H_1(4)| + |H_0(5)| + |H_0(6)| + |H_0(7)|.$$

This means that the subcarriers for the 0th user are assigned in $k = 1, 5, 6$, and 7, and the subcarriers for the 1st user are assigned in $k = 0, 2, 3$, and 4. As a result, the subcarriers for each user are assigned fairly. And then, the MUDiv gain is obtained since the subcarriers for each use are assigned in the good channel condition. The individual subcarrier allocation for $B = 1$ gives the good BER performance, but large computational complexity is required compared with $B > 1$. To solve this problem, the block subcarrier allocation for $B > 1$ is also considered. In the block subcarrier allocation, the block consists of several adjacent subcarriers as

$$\mathcal{H}_{B,u}(k) = \sum_{b=0}^{B-1} H_u(Bk + b). \tag{16}$$

In this case, at the example of Fig. 2b, c, J_B for $B = 2$ and 4 is given by

$$\begin{aligned} J_2 =& |\mathcal{H}_{2,1}(0)| + |\mathcal{H}_{2,1}(1)| + |\mathcal{H}_{2,0}(3)| + |\mathcal{H}_{2,0}(4)| \\ =& |H_1(0)| + |H_1(1)| + |H_1(2)| + |H_1(3)| + |H_0(4)| + |H_0(5)| + |H_0(6)| + |H_0(7)|, \\ J_4 =& |\mathcal{H}_{4,1}(0)| + |\mathcal{H}_{4,0}(1)| \\ =& |H_1(0)| + |H_1(1)| + |H_1(2)| + |H_1(3)| + |H_0(4)| + |H_0(5)| + |H_0(6)| + |H_0(7)|. \end{aligned}$$

These mean that the subcarriers for the 0th user are assigned in $k = 4$ to 7, and the subcarriers for the 1st user are assigned in $k = 0$ to 3. From Eqs. (14) and (16), the block subcarrier allocation for $B > 1$ is assigned for the subcarriers of each user, and the MUDiv gain is also obtained. Moreover, the computational complexity for $B > 1$ is reduced compared with $B = 1$.

3.2 Interleaved block subcarrier allocation

As shown in Sect. 3.1, the MUDiv gain is obtained by using the individual and block subcarrier allocations. However, the MUDiv gain for $B > 1$ is to be small since the possibility for the selection of the deep faded subcarrier channel is to be high compared with $B = 1$. Therefore, in the conventional individual and block subcarrier allocations, a trade-off problem is occurred between the MUDiv gain and the computational complexity. Therefore, we propose the interleaved block subcarrier allocation, and its flowchart is indicated in Fig. 3. In the interleaved block subcarrier allocation, the subcarriers for each user are assigned alternately to avoid a deep faded channel, and the block consists of the interleaved subcarrier channel to obtain the MUDiv gain as

$$\begin{aligned} K_I =& \max\left(\sum_{\alpha=0}^{\lfloor N_c/B_{\max}\rfloor N_u - 1} K_{I,\alpha}\right) = \max\left(\sum_{u=0}^{N_u-1}\sum_{k=0}^{\lfloor N_c/B_{\max}\rfloor - 1} |\tilde{\mathcal{H}}_{I,u}(k)|\gamma_u(k)\right) \\ \le& \sum_{u=0}^{N_u-1}\sum_{k=0}^{\lfloor N_c/B_{\max}/N_u - 1\rfloor} |\tilde{\mathcal{H}}_{I,u}^{\max}(k)|, \end{aligned} \tag{17}$$

where

$$\tilde{\mathcal{H}}_{I,u}(k) = \sum_{i'=0}^{I} H_u(I\lfloor N_c/B_{\max}\rfloor k + i'), \tag{18}$$

$\tilde{\mathcal{H}}_{I,u}^{\max}(k)$ is the subcarrier block channel which sorts the power of $\tilde{\mathcal{H}}_{I,u}(k)$ as $|\tilde{\mathcal{H}}_{I,u}^{\max}(0)| \ge \cdots \ge |\tilde{\mathcal{H}}_{I,u}^{\max}(\lfloor N_c/B_{\max}\rfloor - 1)|$. Observing Eq. (17), the interleaved block subcarrier allocation is only achieved in $B = B_{\max}$. And then, in this paper, $B_{\max}$ equals to $\tilde{N}_c$. In this case, at the example of Fig. 4a, K_I for $I = 1$ is given by

$$\begin{aligned} K_1 =& |\tilde{\mathcal{H}}_{1,1}(0)| + |\tilde{\mathcal{H}}_{1,0}(1)| \\ =& |H_1(0)| + |H_0(1)| + |H_1(2)| + |H_0(3)| + |H_1(4)| + |H_0(5)| + |H_1(6)| + |H_0(7)|. \end{aligned}$$

This means that the subcarriers for the 0th user are assigned in $k = 1, 3, 5$, and 7, and the subcarriers for the 1st user are assigned in $k = 0, 2, 4$, and 6. Therefore, in the proposed method, the subcarriers for each user are assigned alternately with the MUDiv gain in the frequency band. Moreover, in this paper, we consider also the case of $I > 1$. This is achieved by using Eq. (18), and the interleaved block consists of several subcarriers. And then, the subcarriers for each user are assigned as shown in Fig. 4b. In this case, K_I for $I = 2$ is given by

$$\begin{aligned} K_2 =& |\tilde{\mathcal{H}}_{2,1}(0)| + |\tilde{\mathcal{H}}_{2,0}(1)| \\ =& |H_1(0)| + |H_1(1)| + |H_0(2)| + |H_0(3)| + |H_1(4)| + |H_1(5)| + |H_0(6)| + |H_0(7)|. \end{aligned}$$

This means that the subcarriers for the 0th user are assigned in $k = 2, 3, 6$, and 7, and the subcarriers for the 1st user are assigned in $k = 0, 1, 4$, and 5. Therefore, in the proposed method, the subcarriers of each user for $I > 1$ are also assigned.

3.3 Interleaved block subcarrier allocation and power combination

In a FSS-OFDM, the OFDM symbols are spread as shown in Eq. (6). In this case, the power of each subcarrier is different in the frequency band as shown in Fig. 5. Moreover, as the above mentioned, the channel is also fluctuated in the frequency band. By using these characteristics, the power combination between the subcarrier and the channel has been proposed. In this paper, we propose the interleaved block subcarrier allocation and the power combination, and its flowchart is indicated in Fig. 3.

As shown in Sects. 3.1 and 3.2, when the subcarriers for each user are assigned, the utilized frequency is also determined by Eq. (17). Here, the assigned channel responses are defined by the matrix form as

$$\mathbf{H}_u^{\mathrm{sel}} = \left[H_u^{\mathrm{sel}}(0), \ldots, H_u^{\mathrm{sel}}(\tilde{N}_{\mathrm{c}} - 1) \right]^{\mathrm{T}}, \tag{19}$$

where $H_u^{\mathrm{sel}}(k) = H_u(k)\gamma_u(k)$ for $\gamma_u(k) = 1$. Next, the selected channel response matrix for Eq. (19) and the spread signal matrix of the ith symbol for Eq. (6) are sorted based on these powers as

$$\mathbf{H}_u^{\mathrm{pow}} = \left[H_u^{\mathrm{pow}}(0), \ldots, H_u^{\mathrm{pow}}(\tilde{N}_{\mathrm{c}} - 1) \right]^{\mathrm{T}}, \tag{20}$$

$$\mathbf{S}_u^{\mathrm{pow}}(i) = \left[s_u^{\mathrm{pow}}(0, i), \ldots, s_u^{\mathrm{pow}}(\tilde{N}_{\mathrm{c}} - 1, i) \right]^{\mathrm{T}}, \tag{21}$$

where $H_u^{\mathrm{pow}}(k)$ is the channel response for $|H_u^{\mathrm{pow}}(0)| \le |H_u^{\mathrm{pow}}(1)| \le \cdots \le |H_u^{\mathrm{pow}}(\tilde{H}_{\mathrm{c}} - 1)|$, and $s_u^{\mathrm{pow}}(k, i)$ is the spread signal for $|s_u^{\mathrm{pow}}(0, i)| \le |s_u^{\mathrm{pow}}(1, i)| \le \cdots \le |s_u^{\mathrm{pow}}(\tilde{H}_{\mathrm{c}} - 1, i)|$. In the proposed method, since the kth largest power for the channel and the subcarrier is combined, the spread signals for Eq. (21) are mapped in the frequency band based on Eq. (20) as

$$m_u^{\mathrm{pow}}(k, i) = \begin{cases} s_u^{\mathrm{pow}}(k, i) & \text{for } H_u^{\mathrm{pow}}(k) = \sum_{k'}^{N_{\mathrm{c}}-1} H_u(k')\gamma_u(k) \text{ and } \gamma_u(k) = 1 \\ 0 & \text{for } \gamma_u(k) = 0. \end{cases} \tag{22}$$

In this case, at the example of Fig. 5, $H_u^{\mathrm{pow}}(k)$ is given by

$$H_0^{\mathrm{pow}}(0) = H_0(3),\ H_0^{\mathrm{pow}}(1) = H_0(5),\ H_0^{\mathrm{pow}}(2) = H_0(1),\ H_0^{\mathrm{pow}}(3) = H_0(7),$$

$$H_1^{\mathrm{pow}}(0) = H_1(2),\ H_1^{\mathrm{pow}}(1) = H_1(6),\ H_1^{\mathrm{pow}}(2) = H_1(0),\ H_1^{\mathrm{pow}}(3) = H_1(4).$$

Moreover, $s_u^{\mathrm{pow}}(k,i)$ is given by

$$s_0^{\mathrm{pow}}(0,i) = s_0(1,i),\ s_0^{\mathrm{pow}}(1,i) = s_0(3,i),\ s_0^{\mathrm{pow}}(2,i) = s_0(2,i),\ s_0^{\mathrm{pow}}(3,i) = s_0(0,i),$$

$$s_1^{\mathrm{pow}}(0,i) = s_1(3,i),\ s_1^{\mathrm{pow}}(1,i) = s_1(0,i),\ s_1^{\mathrm{pow}}(2,i) = s_1(2,i),\ s_1^{\mathrm{pow}}(3,i) = s_1(1,i).$$

In this case, if $k = 0$, 2, 4, and 6, $m_0^{\mathrm{pow}}(k,i) = 0$. Otherwise, $m_0^{\mathrm{pow}}(k,i)$ is assigned as

$$m_0^{\mathrm{pow}}(1,i) = s_0^{\mathrm{pow}}(2,i) = s_0(2,i) \quad \text{for } H_0^{\mathrm{pow}}(2) = H_0(1),$$

$$m_0^{\mathrm{pow}}(3,i) = s_0^{\mathrm{pow}}(0,i) = s_0(1,i) \quad \text{for } H_0^{\mathrm{pow}}(0) = H_0(3),$$

$$m_0^{\mathrm{pow}}(5,i) = s_0^{\mathrm{pow}}(1,i) = s_0(3,i) \quad \text{for } H_0^{\mathrm{pow}}(1) = H_0(5),$$

$$m_0^{\mathrm{pow}}(7,i) = s_0^{\mathrm{pow}}(3,i) = s_0(0,i) \quad \text{for } H_0^{\mathrm{pow}}(3) = H_0(7).$$

Similarly, if $k = 1$, 3, 5, and 7, $m_1^{\mathrm{pow}}(k,i) = 0$. Otherwise, $m_1^{\mathrm{pow}}(k,i)$ is assigned as

$$m_1^{\mathrm{pow}}(0,i) = s_1^{\mathrm{pow}}(2,i) = s_1(2,i) \ \text{ for } H_1^{\mathrm{pow}}(2) = H_1(0),$$

$$m_1^{\mathrm{pow}}(2,i) = s_1^{\mathrm{pow}}(0,i) = s_1(3,i) \ \text{ for } H_1^{\mathrm{pow}}(0) = H_1(2),$$

$$m_1^{\mathrm{pow}}(4,i) = s_1^{\mathrm{pow}}(3,i) = s_1(1,i) \ \text{ for } H_1^{\mathrm{pow}}(3) = H_1(4),$$

$$m_1^{\mathrm{pow}}(6,i) = s_1^{\mathrm{pow}}(1,i) = s_1(0,i) \ \text{ for } H_1^{\mathrm{pow}}(1) = H_1(6).$$

Therefore, the proposed method achieves the interleaved block subcarrier allocation and the power combination based on Eq. (22).

3.4 Computational complexity for conventional and proposed subcarrier block allocations

In this Section, we indicate the computational complexity for the conventional and proposed block subcarrier allocations. Firstly, the computational complexity for the individual and block subcarrier allocations for Eq. (14) is given by

$$C_{\mathrm{blo}} = \left\lfloor \frac{N_{\mathrm{c}}}{B} \right\rfloor^{N_{\mathrm{u}}}. \tag{23}$$

Next, the interleaved block subcarrier allocation for Eq. (17) is only achieved in $B = B_{\max}$, and $\lfloor N_{\mathrm{c}}/B_{\max} \rfloor$ equals to N_{u}. Therefore, the computational complexity for the interleaved block subcarrier allocation is given by

$$C_{\mathrm{int}} = \left\lfloor \frac{N_{\mathrm{c}}}{B_{\max}} \right\rfloor^{N_{\mathrm{u}}} = N_{\mathrm{u}}^{N_{\mathrm{u}}}. \tag{24}$$

Finally, the power combination for Eq. (22) is achieved after the utilized frequency selection for each user based on Eq. (17). Therefore, the computational complexity for the power combination is given by

Table 3 Computer simulation parameters

Data modulation	16QAM
Data detection	ZF, MMSE
Symbol duration	10 μs
Number of data symbols	20
Number of users	4
Number of data subcarriers	128
FFT size	128
WHT and DFT spreading length	32
Guard interval	32 sample time
Path model	15 path Rayleigh fading
Doppler frequency	5 Hz
Channel estimation	Perfect
FEC	Convolutional code for $(R, K) = (1/2, 7)$

Table 4 Path model

Tap	Delay (sample time)	Average power (dB)
1	0	0
2	1	− 1
3	2	− 2
4	3	− 3
5	4	− 4
6	5	− 5
7	6	− 6
8	7	− 7
9	8	− 8
10	9	− 9
11	10	− 10
12	11	− 11
13	12	− 12
14	13	− 13
15	14	− 14

$$C_{\mathrm{pow}} = \left\lfloor \frac{N_{\mathrm{c}}}{B_{\max}} \right\rfloor^{N_{\mathrm{u}}} + (2\tilde{N}_{\mathrm{c}}^2 + N_{\mathrm{c}})N_{\mathrm{d}} = N_{\mathrm{u}}^{N_{\mathrm{u}}} + (2\tilde{N}_{\mathrm{c}}^2 + N_{\mathrm{c}})N_{\mathrm{d}}. \tag{25}$$

In Sect. 4, we will compare these computational complexities by using the computer simulation parameter of Table 3.

4 Results and discussion

In this section, we discuss the system performance for the conventional and proposed methods by using the computer simulation. Table 3 shows the computer simulation parameters. In this simulation, we assume FSS-MUDiv/OFDMA systems for $N_{\mathrm{u}} = 4$. And then, in the propagation channel, the symbol duration is 10 μs, the GI length is 2 μs, and the path model is 15 path Rayleigh fading at Doppler frequency of 5 Hz. Moreover,

Table 5 Computational complexity for the individual and block subcarrier allocations, the interleaved block subcarrier allocation, and the power combination

B	1	2	4	8	16	32
C_{blo}	268,435,456	16,777,216	1,048,576	65,536	4096	256
C_{int}	–	–	–	–	–	256
C_{pow}	–	–	–	–	–	11,776

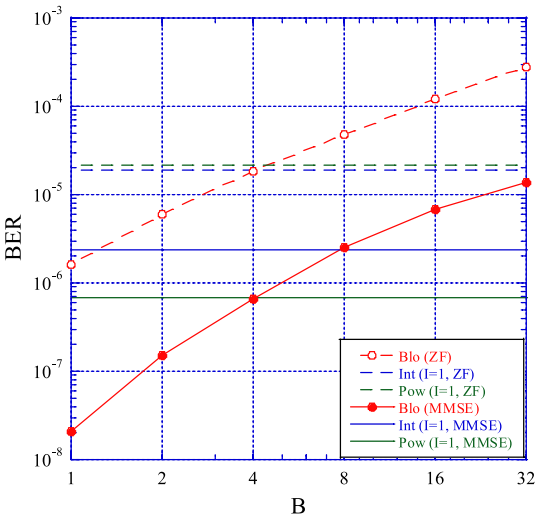

Fig. 6 BER of the various B for the individual and block subcarrier allocations, the interleaved block subcarrier allocation, and the power combination with the DFT, the ZF, and the MMSE, without the coding at $E_b/N_0 = 25$ dB

the path model is indicated in Table 4. Firstly, at the transmitter as shown in Fig. 1a, the original data signals are coded by the convolutional code for $(R, \mathcal{K}) = (1/2, 7)$ with the bit interleaving. After the S/P conversion, the parallel signals are modulated by 16QAM and are spread per the OFDM symbol by the WHT or the DFT. The spread signals for each user are assigned in the frequency band. Here, in the proposed method, the subcarriers for each user are assigned by the interleaved block subcarrier allocation and the power combination. And then, the mapped signals are converted to the time domain signal by the IFFT operation. Finally, after the GI insertion and the P/S conversion, the time domain signal is sent to the receiver via the propagation channel. Next, at the receiver as shown in Fig. 1b, after the S/P conversion and the GI elimination, the time domain signal is converted to the frequency domain signal by the FFT operation. The frequency domain signals are detected by the ZF or the MMSE. Here, we assume the perfect channel estimation. Moreover, the detected signals are demapped and are despread by the WHT or the IDFT. Finally, after the 16QAM demodulation, the demodulated signals are decoded by the Viterbi soft decoding algorithm with the deinterleaving and are returned to the binary signals.

4.1 BER and computational complexity for various *B*

Figure 6 shows the BER of the various B for the individual and block subcarrier allocations, the interleaved block subcarrier allocation, and the power combination with the DFT, the ZF, and the MMSE, without the coding at $E_b/N_0 = 25$ dB. Here, we define that "Blo" is the individual and block subcarrier allocations, "Int" is the interleaved block subcarrier allocation, and "Pow" is the power combination. And then, Table 5 shows the computational complexity for the individual and block subcarrier allocations, the interleaved block subcarrier allocation, and the power combination. In Table 5, they are calculated from Eqs. (23) to (25) by using the parameter of Table 3.

4.1.1 Results

In the ZF case, the block subcarrier allocation for $B = 4$ and the interleaved block subcarrier allocation for $I = 1$ show the same BER performance. Next, in the MMSE case, the block subcarrier allocation for $B = 4$ and the power combination for $I = 1$ show the same BER performance. Moreover, the block subcarrier allocation for $B = 8$ and the interleaved block subcarrier allocation for $I = 1$ show the same BER performance. Also, in all methods, the MMSE shows the good BER performance compared with the ZF.

4.1.2 Discussion

In the ZF case, the computational complexity for the interleaved block subcarrier allocation is reduced to $256/1{,}048{,}576 = 0.0002$ times compared with the block subcarrier allocation for $B = 4$, and they show the same BER performance. Next, in the MMSE case, the computational complexity for the power combination is reduced to $11{,}776/1{,}048{,}576 = 0.0112$ times compared with the block subcarrier allocation for $B = 4$, and they also show the same BER performance. Moreover, the computational complexity for the interleaved block subcarrier allocation is reduced to $256/65{,}536 = 0.0039$ times compared with the block subcarrier allocation for $B = 8$, and they also show the same BER performance. Additionally, the method for the MMSE obtains the good BER performance compared with the ZF since the detected error is reduced by using the noise power and the spreading technique. Therefore, since the proposed method reduces the computational complexity for the subcarrier allocation dramatically and obtains the good BER performance, it solves the trade-off problem for the conventional method.

4.2 BER for various *I*

Figure 7 shows the BER of the various I for the interleaved block subcarrier allocation and the power combination with the WHT, the DFT, the ZF, and the MMSE, without the coding at $E_b/N_0 = 25$ dB. Here, the interleaved block subcarrier allocation for $I = 32$ equals to the block subcarrier allocation for $B = 32$.

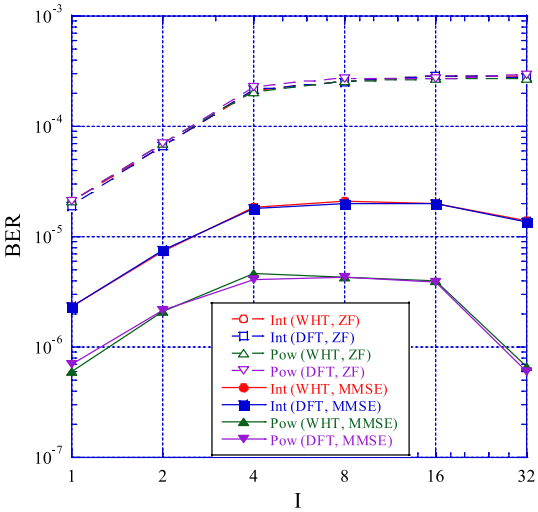

Fig. 7 BER of the various *I* for the interleaved block subcarrier allocation and the power combination with the WHT, the DFT, the ZF, and the MMSE, without the coding at $E_b/N_0 = 25$ dB

4.2.1 Results

When I is small, the interleaved block subcarrier allocation for the ZF and the MMSE, and the power combination for the ZF show the good BER performance. On the other hand, they show the floor in $B \geq 4$. Next, the power combination for the MMSE shows the good BER performance in $I = 1$ and $I = 32$, and they show the same BER performance. Also, in all methods, the MMSE shows the good BER performance compared with the ZF same as the case of Fig. 6. Finally, since the interleaved block subcarrier allocation and the power combination for the WHT and the DFT show the same BER performance.

4.2.2 Discussion

The interleaved block subcarrier allocation and the power combination for $I = 1$ achieve the good BER performance in the ZF and MMSE cases. This means that they are effect when the one chunk length for interleaved block subcarrier allocation (I) is small. And then, they have large effect for the avoiding of continuous deep faded subcarrier channels. Moreover, since their methods with the WHT for the biphase code and the DFT for the polyphase code show the same BER performance, they give the same effect for the BER performance. Additionally, the method for the MMSE obtains the good BER performance compared with the ZF as shown in Section 4.1.2. The advantage of the WHT is the simple processing by the biphase code, and the advantage of the DFT is the low PAPR by the polyphase code [7]. As a result, if the fast processing is required, WHT is better. Also, if the low PAPR is required, DFT is better. Therefore, the proposed method for the WHT and the DFT is effective in a small I.

4.3 BER various E_b/N_0 without coding

Figures 8 and 9 show the BER of the various E_b/N_0 for the interleaved block subcarrier allocation, the power combination, and the WF, with the DFT and the ZF, without the

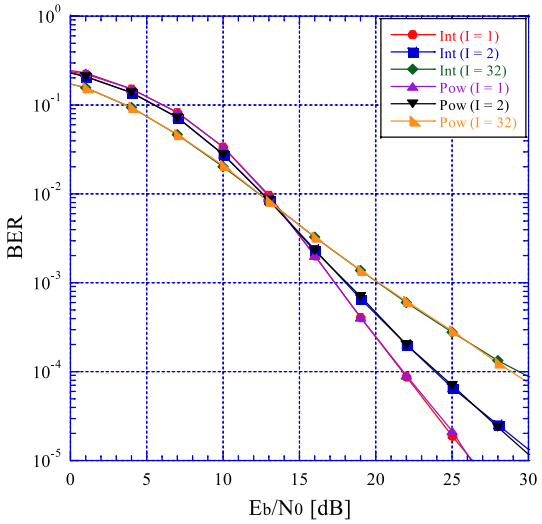

Fig. 8 BER of the various E_b/N_0 for the interleaved block subcarrier allocation and the power combination with the DFT and the ZF, without the coding

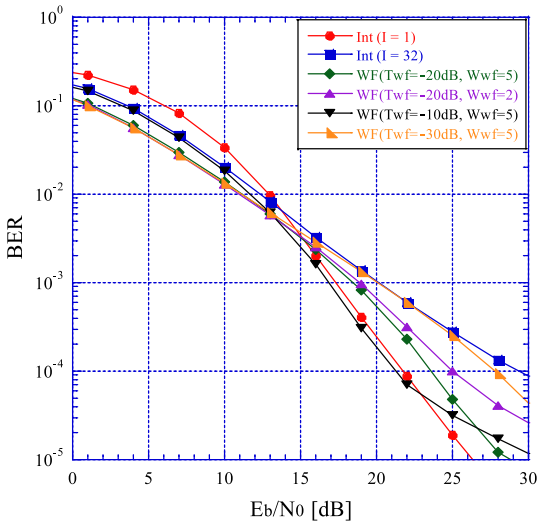

Fig. 9 BER of the various E_b/N_0 for the interleaved block subcarrier allocation and the WF with the DFT and the ZF, without the coding

coding. For the WF method, we assume only the simple method in a MUDiv-OFDMA without the spreading technique. In this case, the method for the ZF and the MMSE shows the same BER performance [25]. Therefore, we show only the ZF case in Fig. 9. The modulated signal between the kth subcarrier and the ith symbol for the uth user after the WF is defined by

$$m_u^{wf}(k,i) = \begin{cases} W_{\mathrm{wf}} m_u(k,i) & \text{for } T_{\mathrm{wf}} > |H_u(k)| \\ m_u(k,i) & \text{for otherwise.} \end{cases} \tag{26}$$

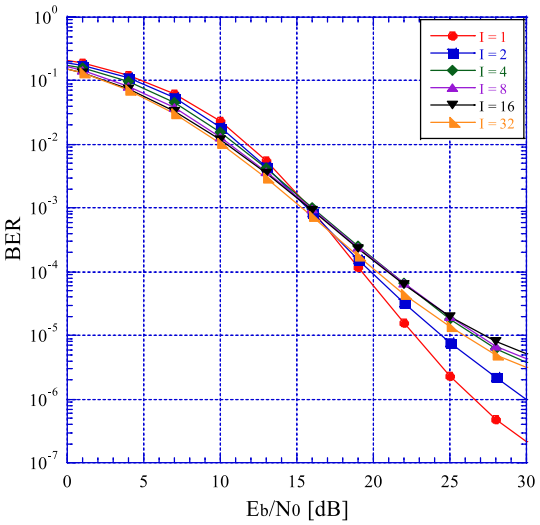

Fig. 10 BER of the various E_b/N_0 for the interleaved block subcarrier allocation with the DFT and the MMSE, without the coding

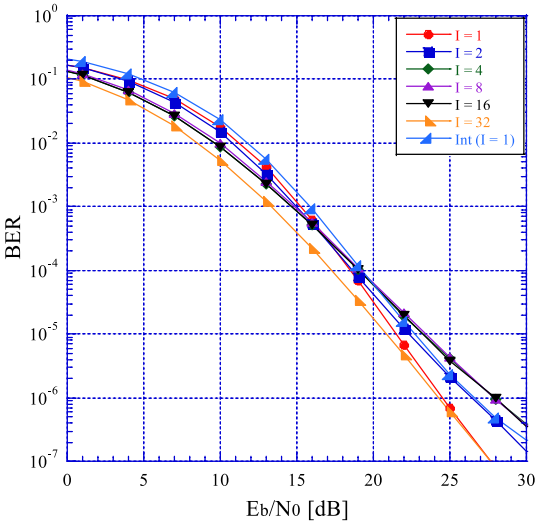

Fig. 11 BER of the various E_b/N_0 for the power combination with the DFT and the MMSE, without the coding

And then, Figs. 10 and 11 show the BER of the various E_b/N_0 for the interleaved block subcarrier allocation and the power combination with the DFT and the MMSE, without the coding. In Fig. 11, the interleaved block subcarrier allocation for $I = 1$ is also shown to compare the power combination.

4.3.1 Results

From the ZF case of Fig. 8, the interleaved block subcarrier allocation for $I = 1$ shows about 4.5 dB gain compared with $I = 2$ in the BER of 1.5×10^{-5}. And then, the interleaved block subcarrier allocation for $I = 2$ shows about 5.5 dB gain compared with $I = 32$ in the BER of 8×10^{-5}. The power combination shows also the same trend,

but the interleaved block allocation and the power combination show the same BER performance in $I = 1$, 2, and 32 as shown in Fig. 7. Next, from Fig. 9, the WF for $T_{\mathrm{wf}} = -20$ dB and $W_{\mathrm{wf}} = 5$ shows about 2 dB gain performance compared with $T_{\mathrm{wf}} = -10$ dB and $W_{\mathrm{wf}} = 5$ in the BER of 1.5×10^{-5} and shows about 3 and 5 dB gain compared with $T_{\mathrm{wf}} = -20$ dB and $W_{\mathrm{wf}} = 2$, and $T_{\mathrm{wf}} = -30$ dB and $W_{\mathrm{wf}} = 5$ in the BER of 4.5×10^{-5}. Moreover, it shows about 6 dB gain compared with the interleaved block subcarrier allocation for $I = 32$. On the other hand, it shows about 3 dB penalty compared with the interleaved block subcarrier allocation for $I = 1$.

From the MMSE case of Fig. 10, the interleaved block subcarrier allocation for $I = 1$ shows about 3.5 dB gain compared with $I = 2$ in the BER of 1×10^{-6} and shows about 6 dB gain compared with $I \geq 4$ in the BER of 3×10^{-6}. Moreover, in the BER of 3×10^{-6}, the interleaved block subcarrier allocation for $I = 2$ shows about 3 dB gain compared with $I \geq 4$, and the interleaved block subcarrier allocation for $I \geq 4$ shows the same BER performance. Moreover, from Fig. 11, the power combination for $I = 1$ shows about 3 dB gain compared with $I = 2$ in the BER of 3×10^{-7} and shows about 4 dB gain compared with $I = 4$, 8 and 16 in the BER of 4×10^{-7}. On the other hand, the power combination for $I = 1$ and 32 shows the same performance in the BER of 1×10^{-7}. Also, the power combination for $I = 2$ and the interleaved block subcarrier allocation for $I = 1$ also show the same performance in the BER of 4×10^{-7}. Additionally, from Figs. 8, 10, and 11, the MMSE shows the good BER performance compared with the ZF in all methods same as the case of Figs. 6 and 7.

4.3.2 Discussion

From the ZF case of Fig. 8, the interleaved block allocation and the power combination show the good BER performance in a small I at various E_{b}/N_0. This reason is discussed in Sect. 4.2.2. However, they show the same BER performance. This means that the influence of the detected error due to the ZF is strong compared with the diversity gain for the power combination. Next, from Fig. 9, the WF for $T_{\mathrm{wf}} = -20$ dB and $W_{\mathrm{wf}} = 5$ shows the good BER performance compared with the interleaved block subcarrier allocation for $I = 32$ by assigning the adaptive threshold and power. This is because WF is achieved based on the interleaved block subcarrier allocation for $I = 32$ without the spreading. On the other hand, it shows the bad BER performance compared with the interleaved block subcarrier allocation for $I = 1$. This means that the proposed method is mitigated for a deep faded subcarrier channel compared with the WF method. Therefore, the proposed method is effective compared with the WF method.

From the MMSE case of Figs. 10 and 11, the interleaved block allocation and the power combination also show the good BER performance in a small I at various E_{b}/N_0 same as the ZF case. And then, from Fig. 11, since the power combination shows the good BER performance compared with the interleaved block subcarrier allocation, the diversity gain for the power combination is obtained in the MMSE case. Therefore, in the proposed method, MMSE is effective to obtain the diversity gain for the power combination. Moreover, the power combination for $I = 2$ and the interleaved block subcarrier allocation for $I = 1$ show the same BER performance. In this case, the computational complexity for the interleaved block subcarrier allocation is reduced to $256/11776 = 0.0217$ times compared with the power combination from Table 5. Additionally, the method

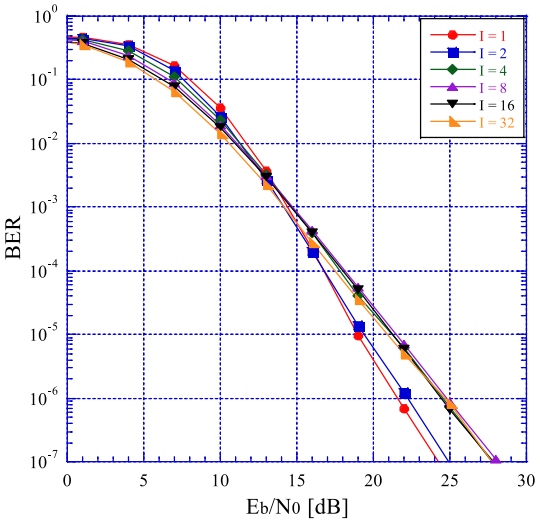

Fig. 12 BER of the various E_b/N_0 for the interleaved block subcarrier allocation with the DFT, the MMSE, and the coding

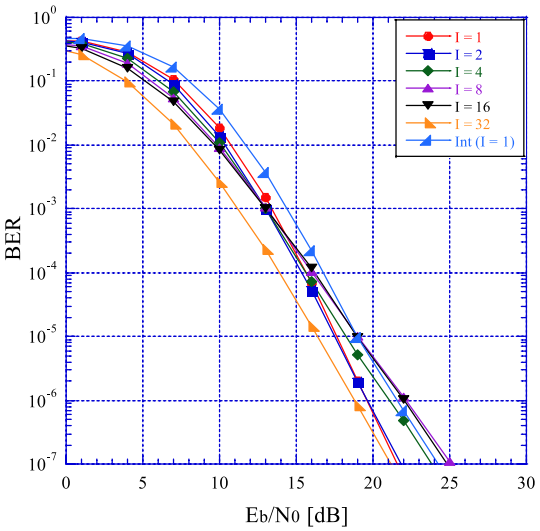

Fig. 13 BER of the various E_b/N_0 for the power combination with the DFT, the MMSE, and the coding

for the MMSE obtains the good BER performance compared with the ZF as shown in Sects. 4.1.2 and 4.2.2. Therefore, the interleaved block subcarrier allocation for $I = 1$ is effective for the BER and the computational complexity in the MMSE case without the coding.

4.4 BER various E_b/N_0 with coding

Figures 12 and 13 show the BER of the various E_b/N_0 for the interleaved block subcarrier allocation and the power combination with the DFT, the MMSE, and the coding.

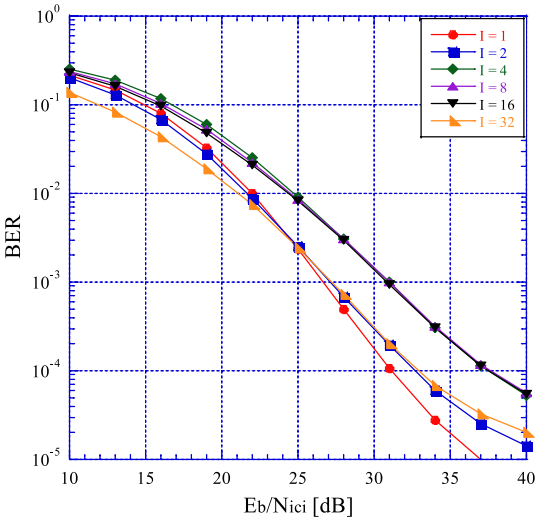

Fig. 14 BER of the various E_b/N_{ici} for the interleaved block subcarrier allocation with the DFT and the MMSE, without the coding at $E_b/N_0 = 25$ dB

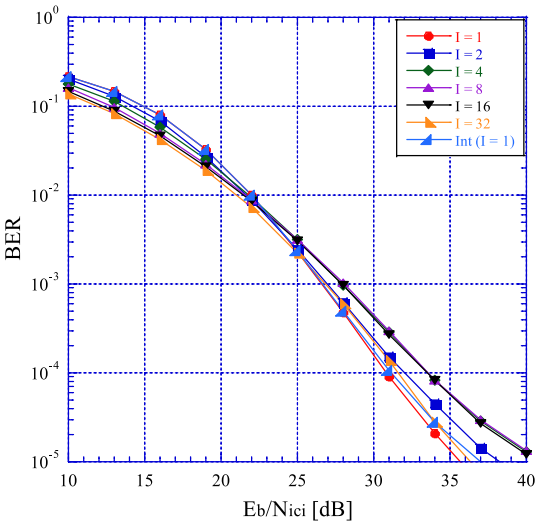

Fig. 15 BER of the various E_b/N_{ici} for the power combination with the DFT and the MMSE, without the coding at $E_b/N_0 = 25$ dB

4.4.1 Results

From Fig. 12, the interleaved block subcarrier allocation for $I = 1$ shows about 1 dB gain compared with $I = 2$ and shows about 4 dB gain compared with $I \geq 4$ in the BER of 1×10^{-7}. Moreover, since the interleaved block subcarrier allocation for $I = 2$ shows about 3 dB gain compared with $I \geq 4$. Next, from Fig. 13, the power combination for $I = 1$, 2, and 32 shows the same performance in the BER of 1×10^{-7}. Moreover, they show about 3 to 4 dB gain compared with $I = 4$, 8, and 16. Also, the interleaved block subcarrier allocation for $I = 1$ also shows the good BER performance same as the power combination for $I = 4$.

4.4.2 Discussion

From Figs. 12 and 13, in the coding case, since the interleaved block subcarrier allocation and power combination for $I = 2$ show the good BER performance, they are effective as $I = 1$. Therefore, the proposed method for $I = 2$ is also effective by obtaining the coding gain. Moreover, since the interleaved block subcarrier allocation for $I = 1$ shows also the good BER performance, it is effective as the uncoding case.

4.5 BER various E_b/N_{ici}

Figures 14 and 15 show the BER of the various E_b/N_{ici} for the interleaved block subcarrier allocation and the power combination with the DFT and the MMSE, without the coding at $E_b/N_0 = 25$ dB.

4.5.1 Results

From Fig. 14, the interleaved block subcarrier allocation for $I = 1$ shows about 4 dB gain compared with $I = 2$ in the BER of 1.5×10^{-5}. And then, it shows about 8 dB gain compared with $I = 4$, 8, and 16 in the BER of 5×10^{-5}. Also, the interleaved block subcarrier allocation for $I = 2$ shows also the good BER performance compared with the $I = 32$ (i.e., the conventional block subcarrier allocation for $B = 32$), but $I = 4$, 8, and 16 show the bad BER performance. Next, from Fig. 15, the power combination for $I = 1$ shows about 1 to 6 dB gain compared with $I = 2$ to 32 in BER of 1×10^{-5}. Moreover, the interleaved block subcarrier allocation for $I = 1$ shows about 1 to 4 dB gain compared with $I = 2$ to 16.

4.5.2 Discussion

From Figs. 14 and 15, the interleaved block subcarrier allocation and the power combination for $I = 1$ and 2 show the good BER performance. Therefore, the proposed method is effective to reduce the influence of the ICI by using the interleaved allocation and the MUDiv gain same as the E_b/N_0 case.

5 Conclusion

In this paper, we have proposed the interleaved block subcarrier allocation and the power combination for a FSS-MUDiv/OFDMA. In the individual and block subcarrier allocations, the MUDiv gain is obtained by using the independent channel fluctuation for each user, but they have a trade-off problem between the BER performance and the computational complexity. To solve this problem, in the proposed method, the interleaved block subcarrier allocation which consists of the interleaved block for the individual and several subcarriers is achieved. Moreover, the power combination between the selected interleaved subcarrier and channel is also achieved. From the computer simulation results, the proposed method reduces the computational complexity and shows the good BER performance. Especially, in the proposed method, the interleaved block subcarrier allocation for $I = 1$ and 2 is effective for the ZF and the MMSE cases with and without the coding.

Abbreviations

AWGN	Additive white Gaussian noise
BER	Bit error rate
CIR	Channel impulse response
CR	Channel response
CSI	Channel state information
DFT	Discrete Fourier transform
FEC	Forward error correction
FFT	Fast Fourier transform
FSS	Frequency symbol spreading
GI	Guard interval
ICI	Inter-cell interference
IDFT	Inverse DFT
IFFT	Inverse FFT
MUDiv	Multiuser diversity
MMSE	Minimum mean square error
NOMA	Non-orthogonal multiple access
OFDM	Orthogonal frequency division multiplexing
OFDMA	OFDM access
OMA	Orthogonal multiple access
PAPR	Peak average power ratio
P/S	Parallel-to-serial
QAM	Quadrature amplitude modulation
SIC	Successive interference cancellation
S/P	Serial-to-parallel
WF	Water filling
WHT	Walsh-Hadamard transform
WLAN	Wireless local area network
ZF	Zero-forcing

Author contributions

YI proposed the idea and approach and involved in writing. TM contributed the confirmation for the approach and draft. Both authors read and approved the current manuscript.

Funding

This work was supported by Japan Society for the Promotion of Science (JSPS) KAKENHI Numbers 18K04145 and 21K04062, and Strategic Information and Communications R&D Promotion Programme (SCOPE) Number JP225008001.

Declarations

Competing interests

The authors declare that they have no competing interests.

Received: 15 August 2021 Accepted: 29 May 2022
Published online: 07 June 2022

References

1. L.J. Cimini, Analysis and simulation of a digital mobile channel using orthogonal frequency division multiplexing. IEEE Trans. Commun. **33**(7), 666–675 (1985)
2. J.J. Gimenez, D.G. Barquero, J. Morgade, E. Stare, Wideband broadcasting: a power-efficient approach to 5G broadcasting. IEEE Commun. Mag. **56**(3), 119–125 (2018)
3. M. Nurchis, B. Bellalta, Target wake time: scheduled access in IEEE 802.11ax WLANs. IEEE Wirel. Commun. **26**(2), 142–150 (2019)
4. L. Zhu, Z. Xiao, X.-G. Xia, D.O. Wu, Millimeter-wave communications with non-orthogonal multiple access for B5G/6G. IEEE Access **7**, 116123–116132 (2019)
5. Z. Wei, J. Guo, D.W.K. Ng, J. Yuan, Fairness comparison of uplink NOMA and OMA, in *IEEE 85th Vehicular Technology Conference* (2017). https://doi.org/10.1109/VTCSpring.2017.8108680
6. M. Munster, L. Hanzo, Performance of SDMA multiuser detection techniques for walsh-hadamard-spread OFDM schemes, in *IEEE 54th Vehicular Technology Conference* (2001). https://doi.org/10.1109/VTC.2001.957162
7. Z. Dong, S. Matsufuji, Y. Ida, T. Matsumoto, A study on PAPR reduction in OFDM using complex hadamard matrices, in *The 8th International Workshop on Signal Design and Its Applications in Communications* (2017), pp. 154–158
8. J. Kim, Y.H. Yun, C. Kim, J.H. Cho, Minimization of PAPR for DFT-spread OFDM with BPSK Symbols. IEEE Trans. Veh. Technol. **67**(12), 11746–11758 (2018)
9. A. Sahin, N. Hosseini, H. Jamal, S.S.M. Hoque, D.W. Matolak, DFT-spread-OFDM-based chirp transmission. IEEE Commun. Lett. **25**(3), 902–906 (2021)
10. F. Adachi, H. Tomeba, K. Takeda, Frequency-domain equalization for broadband single-carrier multiple access. IEICE Trans. Commun. **E92–B**(5), 1441–1456 (2009)

11. T. Svensson, T. Frank, T. Eriksson, D. Aronsson, M. Sternad, A. Klein, Block interleaved frequency division multiple access for power efficiency, robustness, flexibility, and scalability. EURASIP J. Wirel. Commun. Netw. (2009). https://doi.org/10.1155/2009/720973
12. Y. Shao, S.C. Liew, Flexible subcarrier allocation for interleaved frequency division multiple access. IEEE Trans. Wirel. Commun. **19**(11), 7139–7152 (2020)
13. S.C. Liew, Y. Shao, New transceiver designs for interleaved frequency-division multiple access. IEEE Trans. Wirel. Commun. **19**(12), 7765–7778 (2020)
14. Y. Karasawa, H. Iwai, Modeling of signal envelope correlation of line-of-sight fading with applications to frequency correlation analysis. IEEE Trans. Commun. **42**(6), 2201–2203 (1994)
15. C.Y. Wong, R.S. Cheng, K.B. Letaief, R.D. Murch, Multiuser OFDM with adaptive subcarrier, bit, and power allocation. IEEE J. Sel. Areas Commun. **17**(10), 1747–1758 (1999)
16. C. Ahn, D. Har, T. Omori, K. Hashimoto, Frequency symbol spreading based adaptive subcarrier block selection for OFDMA system. Digit. Signal Process. **22**(3), 518–525 (2012)
17. T. Mert, O. Kaya, H. A. Cirpan, Jointly optimal chunk and power allocation in uplink SC-FDMA, in *IEEE International Conference on Communications* (2013), pp. 3393–3397
18. Y. Ida, C. Ahn, T. Matsumoto, S. Matsufuji, Removing deep faded subcarrier channel for cooperative multiuser diversity OFDMA based on low granularity block. IEICE Trans. Fundam. **E97–A**(12), 2586–2594 (2014)
19. C.-H. Choi, H.-J. Kim, T.-K. Kim, G.H. Im, Spectral efficient multiuser technique with channel-dependent resource allocation schemes. IEEE Trans. Wirel. Commun. **11**(3), 990–999 (2012)
20. Y. Ida, T. Matsumoto, S. Matsufuji, Interleaved MUDiv block allocation and optimum power control for SC-FDMA, in *RISP International Workshop on Nonlinear Circuits. Communications and Signal Processing*, vol. 2017 (2017), pp. 517–520
21. A. Kuroha, C. Ahn, T. Omori, K. Hashimoto, Multiuser diversity OFDMA using power priority selection and adaptive clipping. Int. J. Dist. Syst. Technol. **5**(4), 18–30 (2014)
22. T. Iwata, H. Miyazaki, F. Adachi, Capacity-fairness controllable scheduling algorithms for single-carrier FDMA. IEICE Trans. Commun. **E97–B**(7), 1474–1482 (2014)
23. J. Mao, G. Xie, J. Gao, Y. Liu, Energy efficiency optimization for OFDM-based cognitive radio systems: a water-filling factor aided search method. IEEE Trans. Wirel. Commun. **12**(5), 2366–2375 (2013)
24. S. Khakurel, L. Musavian, H.V. Vu, T.L. Ngoc, QoS-aware utility-based resource allocation in mixed-traffic multi-user OFDM systems. IEEE Access **6**, 21646–21657 (2018)
25. Y. Ida, T. Matsumoto, S. Matsufuji, Different antenna interleaved allocation with full and divided WHT/DFT spreading for HTRCI-MIMO/OFDM. IEICE Trans. Commun. **E103–B**(12), 1438–1446 (2020)

Publisher's Note